ADVANCED OPTICAL MATERIALS
www.advopticalmat.de

Microcavity-Enhanced Blue Organic Light-Emitting Diode for High-Quality Monochromatic Light Source with Nonquarterwave Structural Design

*Jie Lin, Yongsheng Hu, and Xingyuan Liu**

Despite their rapid development, organic light-emitting diodes (OLEDs) are limited to display and lighting applications, and exploiting the application and development of OLEDs has become one of the critical issues. In this study, a new type of distributed Bragg reflector (DBR) with low absorption spacer as a bottom mirror is developed through nonquarterwave structural design. Different factors affecting the electroluminescence (EL) properties of microcavity OLEDs (MOLEDs) are investigated by using the optical microcavities with different structures to regulate the EL properties of 4,4′-bis[(N-carbazole)styryl] biphenyl (BSB-Cz). The optimized MOLEDs with quarterwave DBRs exhibited a maximum external quantum efficiency of 8.86 ± 0.06%, demonstrating an enhancement of 79% compared to a reference device. Under the premise of almost not changing the electrical injection of the functional layer materials in the cavity, the spectral full-width at half maximum of MOLEDs with a nonquarterwave structural design is as narrow as 2 ± 0.05 nm. These improvements are not only suitable for small organic molecules or polymeric materials, but also for novel nanoluminescent materials, such as quantum dots, perovskites, etc. Overall, the current study suggests the general applicability of this novel concept to obtain high-quality monochromatic light, irrespective of the type of materials used.

1. Introduction

Significant progress has already been made in organic light-emitting diodes (OLEDs), which gained immense attention both in academia and industry over the last three decades.[1–3] Researchers are focused on the two promising applications of OLEDs: display devices and lighting panels.[4–7] However, further development of OLEDs technology is facing enormous challenges, such as cost, emitter, light extraction, etc.[8,9] On the one hand, in recent years, with the fast progress in performance, newly developed light-emitting devices such as quantum dot light-emitting diodes (QLEDs) have approached the state-of-the-art OLEDs only in one decade. QLEDs have preliminarily become competitive with OLEDs in the field of lighting and display.[10–13] On the other hand, due to the lacking of an adequate new type of organic electroluminescent (EL) devices based on OLEDs, it impedes taking full advantage of the integration of OLEDs with other optoelectronic devices. Therefore, OLEDs technology still has space for development.[14] Many different types of EL technology based on OLEDs have not been well developed. For example, microcavity OLEDs (MOLEDs) have been successfully used as monochrome light in sensors[15–17] or organic semiconductor amplifiers.[18] The full-width at half-maximum (FWHM) of the novel MOLEDs with distributed Bragg reflector (DBR)/indium tin oxide (ITO) less than 7 nm[15] and tunable near UV MOLEDs arrays[16] have been obtained and significant improvements can still be introduced. Compared with the MOLEDs, the current application of resonant cavity light-emitting diodes (RCLEDs) is more like a mature technology,[19,20] which can be used in a variety of low-cost, high-volume applications, especially for optical communication, more specifically, through a plastic optical fiber (POF) and IR wireless communication for data communication.[21,22] The key reasons are the following: 1) the wide spectrum of organic materials makes the angular dispersion of MOLEDs very serious, which would affect the beam quality; 2) the lack of a reasonable resonator structure to control the spontaneous emission characteristics of OLEDs effectively. At present, metal cavities or metal-dielectric cavities are most commonly used in MOLEDs,[23,24] and all-dielectric MOLEDs have also been reported,[25,26] but the overall performance is poor owing to the extra optical loss in the resonator is difficult to control. It is worth noting that constructing a reasonable

Dr. J. Lin, Dr. Y. Hu, Prof. X. Liu
State Key Laboratory of Luminescence and Applications
Changchun Institute of Optics
Fine Mechanics and Physics
Chinese Academy of Sciences
Changchun 130033, China
E-mail: liuxy@ciomp.ac.cn
Prof. X. Liu
Center of Materials Science and Optoelectronics Engineering
University of Chinese Academy of Sciences
Beijing 100049, China
The ORCID identification number(s) for the author(s) of this article can be found under https://doi.org/10.1002/adom.201901421.

DOI: 10.1002/adom.201901421

microcavity is not easy to achieve by adopting the existing structural parameters. Taking metal-dielectric MOLEDs as an example, the large difference in refractive index between high and low dielectric materials determines the variations in the reflectance of conductive dielectric DBR considerably in different periods. While the immobilization of reflectivity of thick metal electrodes further reduces the space for controlling the luminescent properties of OLEDs by microcavity. Therefore, the spectral FWHM of common MOLED is usually between 10 and 20 nm, and the enhancement of external quantum efficiency (EQE) is usually one- to twofold,[27] which is far behind RCLEDs (FWHM, 40–1 nm; EQE enhancement, one- to tenfold). For large area tunable monochrome light source or POF communication, it is necessary to improve the performance of MOLEDs. Although many different approaches to the development of functional materials and devices are designed for improving the performance of blue OLED devices, until now, the efficiency and stability of blue OLEDs still have few concerns.[28] Due to their poor photophysical properties,[29] efficient deep-blue materials are developed gradually until the emergence of thermally activated delayed fluorescence materials.[30] A wide variety of blue luminescent organic materials with excellent photophysical properties has been developed by using reasonable molecular design concepts and general synthetic routes.[31,32] Among them, 4,4′-bis[(N-carbazole)styryl] biphenyl (BSB-Cz) based on the structure of bis-stilbene has excellent photophysical properties, including high photoluminescence quantum yield (PLQY) in solid state, high radiative rate constant (kr, 10^9 S^{-1}), and very low excited-state absorption and thus considered to be a very promising candidate for high-efficiency deep-blue OLEDs. BSB-Cz possesses a high PLQY even in neat films, which is contrary to the strong concentration quenching exhibited by many organic dyes.[33] This characteristic property is advantageous to adjust the natural spontaneous emission by utilizing optical microcavity. It is well known that the optical microcavity can increase the light extraction efficiency of OLED by changing the distribution of light inside the device, producing saturated colors, and improving the color gamut.[24] Unfortunately, EQE of reported blue MOLEDs is lower than the expected, which may be due to a considerable mismatch between the resonant wavelength of the cavity and blue emission spectrum, as the resonant wavelength of the emitted light deviates from the peak value of the intrinsic luminescence, resulting in a lower enhancement of quantum efficiency. Therefore, it is challenging to improve the efficiency of blue OLED while shifting the emission peaks to shorter wavelengths to produce a deeper blue color.

Here, we demonstrate a MOLED that employs a nonquarterwave structural design, possessing tunable spectral FWHM as narrow as 2 ± 0.05 nm. A simple structural design reported here plays two key roles: optimizing electric injection balance and regulating the optical mode. This investigation successfully discusses and addresses these two effects separately. The insights revealed by this study using nonquarterwave MOLEDs help boost the application of MOLEDs. At the same time, it is equally beneficial to facilitate the realization of electrically driven organic lasers in the blue region.

2. Results and Discussion

2.1. High-Performance Blue OLED based on BSB-Cz

To evaluate the EL properties of BSB-Cz, we employed a simple but highly efficient structural device (**Figure 1**a) that consists of multiple layers in the following order: ITO (≈120 nm)-coated glass substrates, molybdenum trioxide (MoO_3 ≈1 nm), 4,4′,4′-*tris*(carbazol-9-yl)-triphenylamine (TCTA ≈40 nm), 4,4′-bis(*N*-carbazolyl)-1,1′-biphenyl (CBP ≈20 nm), 4,4′-bis[(*N*-carbazole)styryl]biphenyl-doped CBP (BSB-Cz:CBP ≈20 nm, 3–15 wt%), 1,3,5-*tris*(*N*-phenylbenzimidazole-2-yl)benzene (TPBI ≈40 nm), lithium fluoride (LiF ≈1 nm), and aluminium electrodes (≈100 nm). An energy level alignment system is adopted for multilayer OLEDs to achieve efficient blue emission (Figure 1b). Such a strategy has been demonstrated in earlier studies, which aim at reducing the height of the barrier at the interface, thereby promoting the equilibrium of carrier injection in the OLEDs.[3] On the one hand, to avoid the formation of hole transport layer (HTL)/emissive layer (EML) interfacial exciplex, HTL material next to EML should have a wider bandgap and lower highest occupied molecular orbital energy level. On the other hand, the deep lowest unoccupied molecular orbital level of electron transport layer (ETL) materials promotes the injection of electrons, which quickly transfer into EML to form excitons with holes in the emissive layer. Such a recombination mechanism, not only suppresses the formation of exciplex on the interfaces of HTL/EML but also provides multiple potential-reducing paths to balance the carrier equilibrium.[34,35] Under this conception, appropriate alignment of energy level in the multilayer OLEDs can be achieved, which improves the luminescent efficiency of the exciton. In order to study the effect of doping concentration on the luminescence properties, devices with five different doping concentrations were fabricated on the glass substrates for blue OLEDs: B1 (3 wt%), B2 (6 wt%), B3 (8 wt%), B4 (12 wt%), and B5 (15 wt%). A typical EL spectrum of the device B4 is illustrated in Figure S1 in the Supporting Information. The EL peak at 462 nm accompanied by a shoulder around 436 nm with a narrow FWHM of 56 nm corresponds to color-saturated blue emission, i.e., with Commission Internationale de l'Eclairage (CIE) color coordinates of (0.15, 0.09), which is close to the standards of National Television System Committee (NTSC) (CIE: 0.14, 0.08) and European Broadcasting Union (EBU) (CIE:0.15, 0.06). Figure 1c shows the characteristics of current density–luminance–voltage (*J*–*L*–*V*) of the blue OLEDs. The *J*–*V* characteristics of all the studied devices are very similar, but the device B4 shows a smaller leakage current compared to other devices, and the current density and luminance increase sharply after the driving voltage is above turn-on voltage (≈3.08 ± 0.04 V). The *L*–*V* curves of the devices also demonstrate similar trends. Notably, device B4 exhibited the highest luminance of 28 600 ± 260 cd cm^{-2} at 12.8 V. The peak and average EQE of B4 and B5 devices are much higher than other devices (Figure 1d), and the peak EQE reaches 5.19 ± 0.05% at 238 cd m^{-2} and 4.55 V, which corresponds to a current efficiency of 5.76 ± 0.06 cd A^{-1}, indicating an enhancement of 20%, 18%, and 10% as compared to

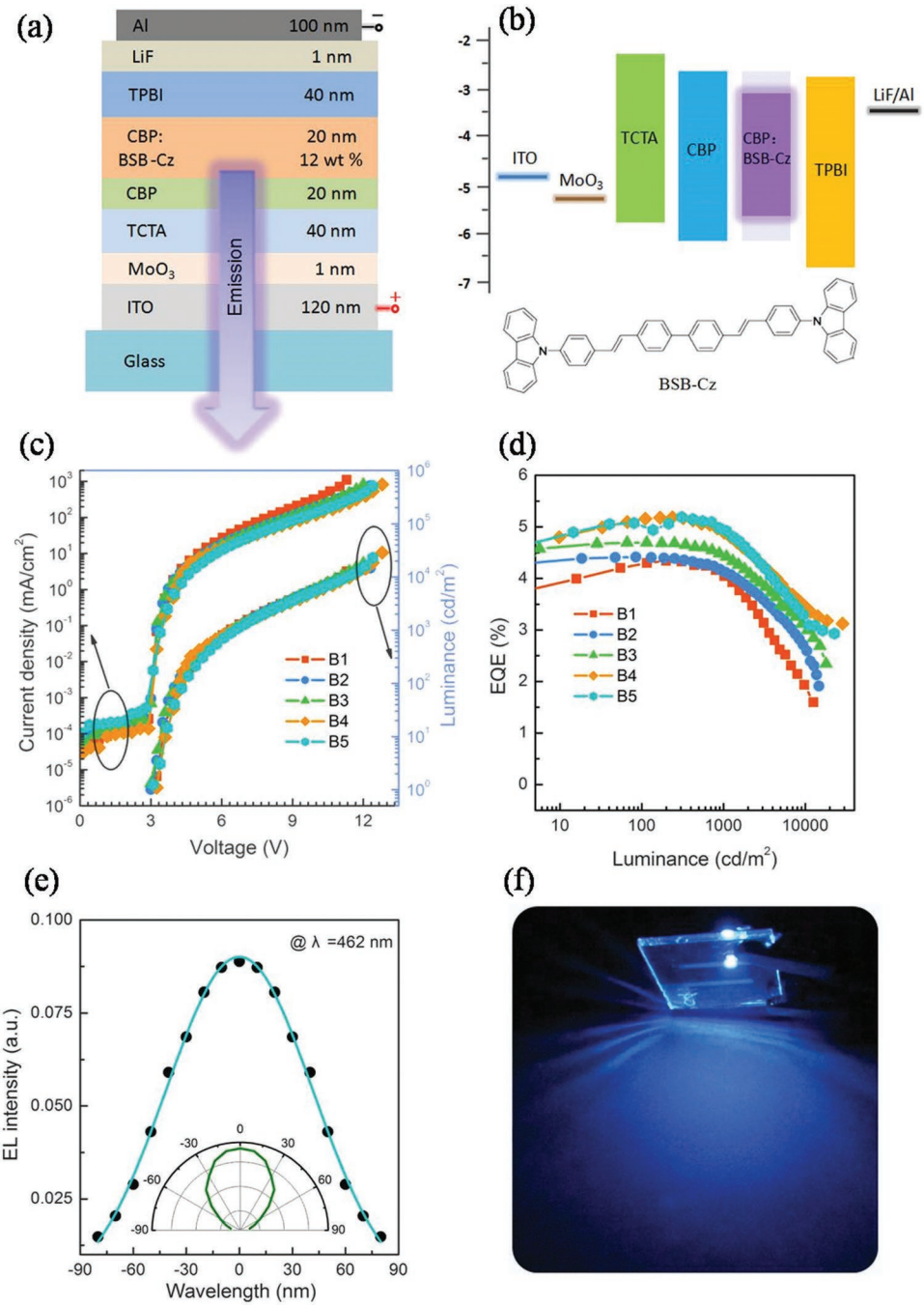

Figure 1. Performances of blue OLEDs with different doping concentrations. a) The optimized devices structure. b) The energy levels of the devices and the structure of BSB-Cz. c) *J*–*L*–*V* characteristics of the devices. d) EQE versus luminance characteristics of the devices. e) The measured EL intensity of OLED as a function of wavelength and observation angle from 0° to 80° with normal direction of substrate. f) Image of B4 device at driving voltage of 8 V.

B1, B2, and B3 devices, respectively. Although the peak EQE of the device B5 is almost the same as that of the B4 device (Table S1, Supporting Information), the EQE of B5 device is 3.09 ± 0.04% at 11 100 cd cm^{-2}, while the EQE of B5 device is 3.36 ± 0.04% under almost the same luminance. The B4 device displays a lower efficiency roll-off than the B5 device. Therefore, the B4 device with a doping concentration of 12% shows the best overall performance, and hence the same doping ratio was used for the latter microcavity devices. The angular emission intensity of the devices is close to the lambertian profile (Figure 1e), and the blue OLEDs show cobalt blue light emitting (Figure 1e). Although the performance of BSB-Cz-based OLEDs is outstanding, owing to their broad half-width spectrum, the wavelength range covers from near-UV to green light. This prevents from directly employing the device for other applications besides lighting and display.

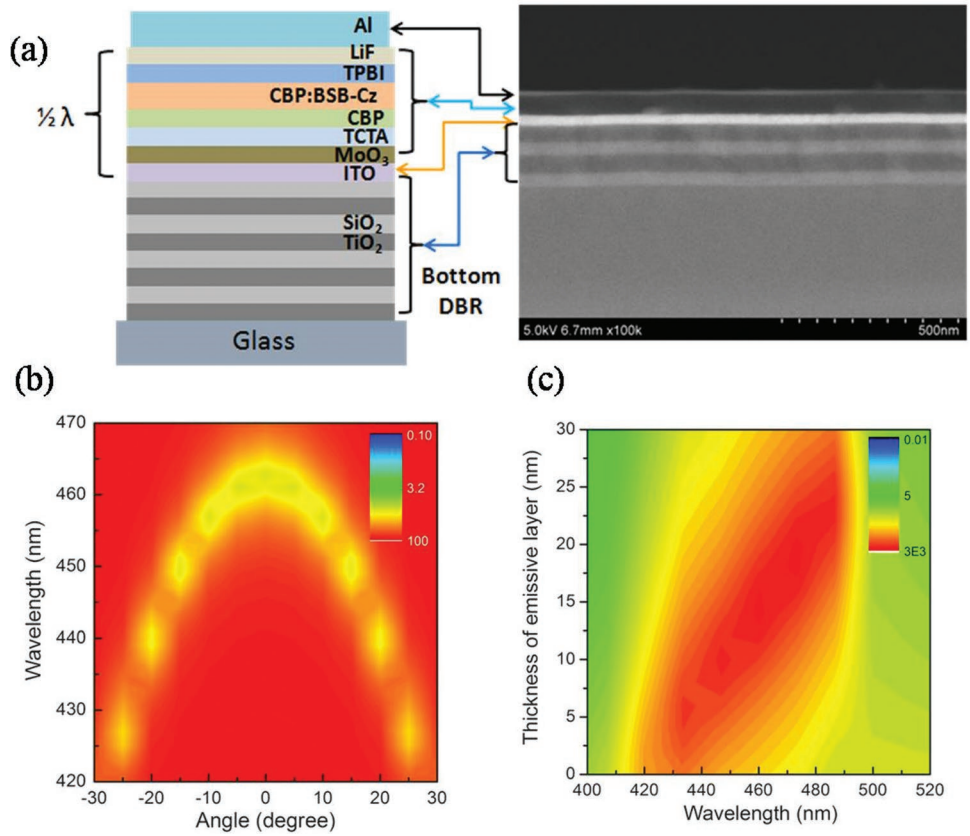

Figure 2. a) The structure diagram and cross-section SEM image of MOLEDs. b) Calculated reflectance intensity of μC B1 device in dependence on the wavelength and the angle θ° relative to the surface normal. c) The theoretical contour plot of the emission intensity in device μC B1 as the function of wavelength and emissive layer thickness.

2.2. Highly Efficient MOLEDs with Quarterwave DBRs

Since the early demonstration of MOLEDs,[36–38] optical microcavity has been widely used in organic optoelectronics to obtain narrow EL spectra of OLEDs with tunable emission wavelength through changing the cavity modes. Optical microcavity can effectively enhance the emission intensity along the normal direction, as well as can reduce the spectral linewidth significantly. Based on the principle of an optical microcavity, it is easy to obtain monochromatic light emission through optical microcavity. The FWHM of microcavity resonance mode is usually smaller than the intrinsic spectrum of the emitter, which effectively enhances the emission.[39] The main purpose of this study is to realize high performance MOLEDs based on high-efficiency BSB-Cz OLEDs. To achieve this, SiO_2/TiO_2 dielectric DBRs were used as the bottom mirror in the fabrication of MOLEDs. This is due to the following reasons: first, dielectric DBR has the advantages of high reflectivity and low absorption properties; second, high reflectivity can be obtained in few periods due to a large difference in the refractive index. To investigate the effect of optical microcavities with different Q values on the EL properties of blue light-emitting materials, MOLEDs were fabricated with DBRs substrates of different reflectivities, and also devices without DBRs as reference. The reference device is B0, while the microcavity (μC) device with quarterwave DBR consists of two pairs of TiO_2/SiO_2 and an ITO layer (DBR1), quarterwave DBR consists of three pairs of TiO_2/SiO_2 and an ITO layer (DBR2), and quarterwave DBR consists of four pairs of TiO_2/SiO_2 and an ITO layer (DBR3), which led to μC B1, μC B2, and μC B3 devices, respectively. To fabricate a reasonable resonator, the emitting layer and multilayered Bragg reflectors must be precisely controlled. **Figure 2**a shows the structural diagram and cross-sectional scanning electron microscope (SEM) image of the μC B1 device. The other cross-sectional SEM images of B0, μC B2, and μC B3 devices are shown in Figure S2 in the Supporting Information. In Figure 2b, the calculated reflectance of the μC B1 device displays typical semi-parabolic cavity mode dispersions in a small angular range. The emission intensity distribution of the μC B1 device is simulated based on the resonance condition of 1/2 λ microcavity and optimized blue OLEDs, which indicate a typical thickness and wavelength dependence (Figure 2c). In an optical microcavity, an increase in the current efficiency and brightness is related to the enhancement factor in the normal direction of the microcavity, while an increase in the EQE is related to the integrated enhancement factor of the microcavity. The resonant emission enhancement factor G_e along the normal direction in a microcavity structure is given by the following Equation (1)[40]

$$G_e = \frac{\xi}{2}\frac{2}{\pi}\frac{\pi(R_1R_2)^{1/4}(1-R_1)}{\left(1-\sqrt{R_1R_2}\right)^2} \quad (1)$$

Whereas, the integrated enhancement factor G_{int} in a microcavity structure is given by the following Equation (2)[40]

$$G_{int} = \frac{\xi}{2}\frac{2}{\pi}\frac{1-R_1}{1-\sqrt{R_1R_2}}\sqrt{\pi \ln 2}\frac{\lambda}{\Delta\lambda_n}\frac{\lambda_{cav}}{L_{cav}}\frac{\tau_{cav}}{\tau} \quad (2)$$

where ξ is the antinode enhancement factor, and λ and λ_{cav} are the emission wavelengths of the active region under vacuum inside the cavity. $\Delta\lambda$ and $\Delta\lambda_n$ are the cavity resonance bandwidth and the natural FWHM of the active medium, respectively. R_1 and R_2 are the reflectivities of the mirrors, L_{cav} is the effective cavity length, L_1 is the effective distance from the emission zone to the first mirror, and t_{cav} and τ are the radiative lifetimes in the cavity and free space, respectively. The antinode enhancement factor ξ is usually between 0 and 2, which depends on the relative position of the active region and standing wave field inside the cavity. Equation (2) also takes into account the changes in the spontaneous emission lifetime in terms of a lifetime without the cavity (τ), as well as the lifetime with the cavity (τ_{cav}). For planar microcavities, τ_{cav}/τ is usually more than 0.9. From this analysis, the relationship between G_e and G_{int} can also be approximately expressed by the following Equation (3)[41]

$$G_{int} = G_e\sqrt{\pi \ln 2}\frac{\Delta\lambda}{\Delta\lambda_n} \quad (3)$$

$\Delta\lambda$ is smaller than $\Delta\lambda_n$ for a resonant cavity and some of the natural emission spectra are strongly enhanced while the remaining spectrum is suppressed. **Figure 3**a shows the *J*–*V*–*L* characteristics of MOLEDs and the reference device. Theoretically, the *J*–*V* characteristic curve of the reference device and microcavity device should be the same, however, although all DBRs used in the experiment were designed and fabricated using electron beam evaporation,[42,43] the same workfunction of ITO in all the DBR batches cannot be achieved due to other parameters, such as ITO storage time, and the ITO electrode pattern process. Owing to the ITO used in the reference B0 device is commercialized and prepared by the magnetron sputtering method, the *J*–*V* curves of the reference B0 device and the microcavity devices (μC B1, μC B2, and μC B3) are significantly different. By continuously optimizing the fabrication process, the *J*–*V* data are very approximated for all the MOLEDs after reaching the turn-on voltage, which is slightly higher than the reference device (B0), showing the highest luminance of 23 000 ± 100 cd m^{-2} at 11.6 V while the luminance of MOLEDs decreases gradually (**Table 1**). The introduction of the luminosity function of human eyes and the microcavity enhancement factor makes it possible that the EQE of microcavity device is higher than that of the reference device even if the luminance of the microcavity device is lower than that of the reference device. Figure 3b displays the EQE for all three devices as a function of luminance, which indicates that the microcavity could assist in suppressing the efficiency roll-off more or less. The maximal EQE for the reference B0 device and μC B1, μC B2, and μC B3 microcavity devices are 4.95 ± 0.05%, 8.86 ± 0.06%, 7.1 ± 0.06%, and 3.18 ± 0.03%, respectively, while μC B1 and μC B2 devices show integrated intensity enhancements of 79% and 43%, respectively, due to the effects of microcavity. The μC B1 device shows the highest enhancement with a resonant wavelength at 462 nm, which corresponds to the closeness of cavity resonance bandwidth to the natural linewidth of the active medium. However, μC B3 was the only device that indicated a decrease in EQE, and μC B1 and μC B2 devices demonstrated noticeable enhancements similar to that of the noncavity B0 device. This may be due to a significant decrease in the cavity resonance bandwidth as the reflectance of DBR3 increases more than 90% at 462 nm. While the μC B1 device shows the highest EQE, and the enhancement ratio of the current efficiency is higher than the quantum efficiency. Figure 3c exhibits the EL spectra of the microcavity devices as well as the EL spectra of the reference device driven at a constant current density. Compared to noncavity devices, MOLEDs show a significant enhancement in the emission intensity along the normal direction with narrow FWHM owing to apparent microcavity effects.[44] The EL peaks of all the optimized MOLEDs are located at 462 nm, which correspond to the resonance mode of the reflectance spectra of the MOLEDs (Figure 3d). For an optical microcavity, the FWHM of the cavity resonance is given by the following Equation (4)

$$\Delta\lambda = \frac{\lambda^2}{2L_{cav}}\left[\frac{1-\sqrt{R_1R_2}}{\pi(R_1R_2)^{1/4}}\right] \quad (4)$$

Based on Equation (4), $\Delta\lambda$ of MOLEDs can be calculated by combining the reflectance spectra of DBR1, DBR2, DBR3, and metal electrode Al (Figure S3, Supporting Information). Theoretically, the calculated $\Delta\lambda$ should be very close to the spectral width of the cavity resonance based on the measured reflectance spectra of MOLEDs and the FWHM of the EL spectra of MOLEDs. The obtained results from theoretical simulations are 16.1, 10.3, and 7.8 nm for μC B1, μC B2, and μC B3 devices, respectively. The EL spectral FWHM of the reference and μC B1, μC B2, and μC B3 devices are 56 ± 1, 18 ± 0.5, 10 ± 0.3, and 8 ± 0.2 nm, respectively, which exhibit a good agreement of EL FWHM between the experimental and theoretical results. The statistical variations of different devices as shown in Table 1 illustrate that the main performance parameters of the devices have low relative standard deviation, which indicated that they have less impact on the performance parameters when dividing by the current device to device variations. The calculated resonant emission enhancement factor (G_e) for μC B1, μC B2, and μC B3 are 5.3, 6.05, and 4.61, respectively. Brightness is closely related to the visual function of human eyes. With the narrowing of the spectral FWHM of the microcavity devices, the contribution of red and green light to the luminance decreases gradually, which is the key reason for a gradual decrease in the luminance of microcavity devices as compared to the reference devices. Based on Equation (3), the integrated enhancement factor (G_{int}) of μC B1, μC B2, and μC B3 devices at an optimized wavelength are 3.40, 5.42, and 3.03, respectively. The CIE coordinates of B0, μC B1, μC B2, and μC B3 devices from EL spectrum are (0.15, 0.09), (0.14, 0.055), (0.16,0. 047), and (0.15, 0.4), respectively, indicating that the emitting color becomes saturated deep blue. Figure 3ef shows the angle dependence of emitting light for the μC B1 device. The MOLEDs show a strong forward emission distribution and blue shift with an increase in the viewing angle. Figure S4 in the Supporting Information exhibits that the microcavity devices have better directionality than noncavity ones.

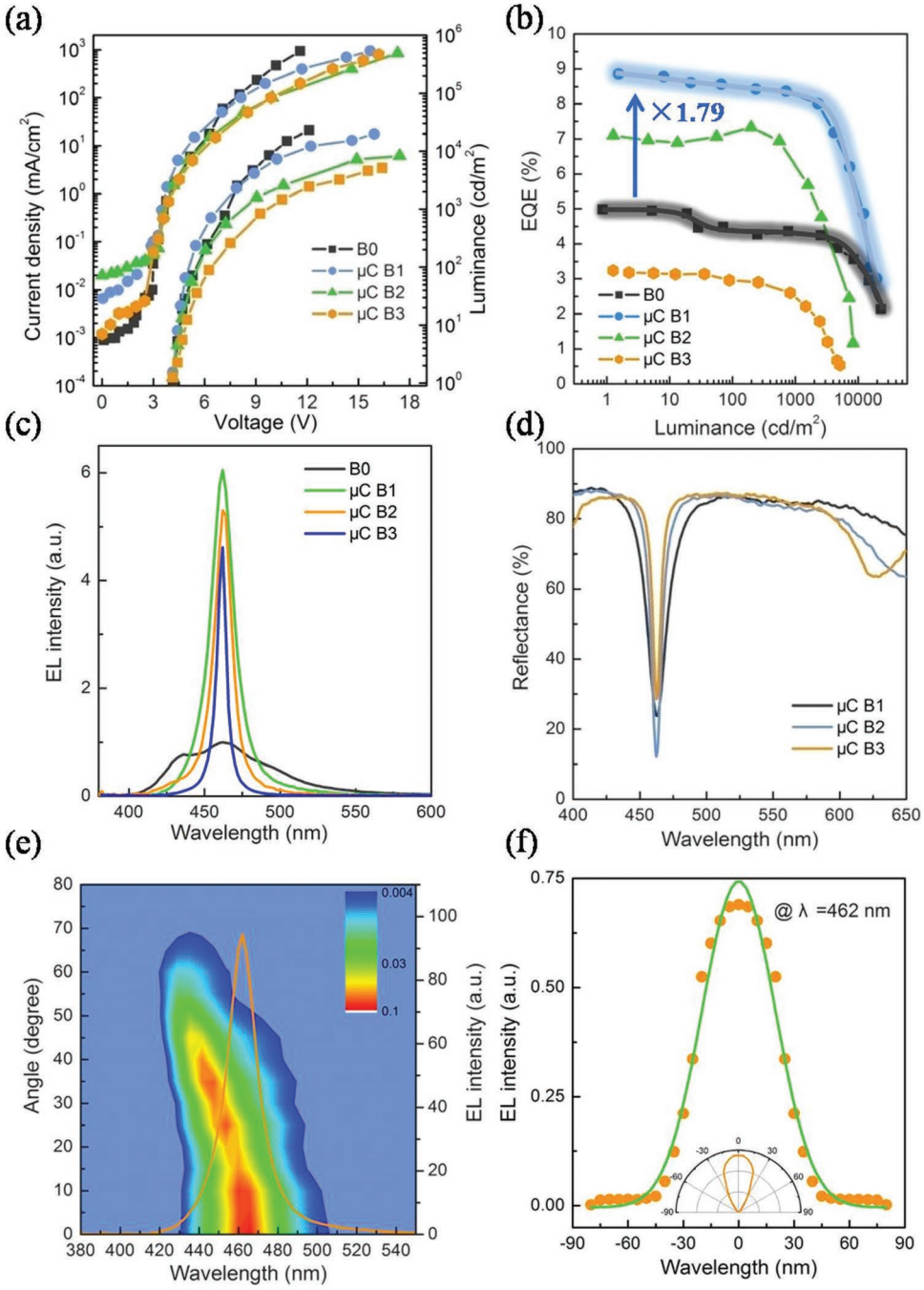

Figure 3. Performance of blue MOLEDs with quarterwave DBRs. a) *J–L–V* characteristics of the devices. b) EQE versus luminance characteristics of the devices. c) EL spectra of device with and without microcavity structure. d) The measured reflectance spectra of MOLEDs with quarterwave DBRs from normal direction of substrate. e) The measured EL intensity of μC B1 device is plotted as a function of wavelength and observation angle from 0° to 80° with normal direction of substrate. f) The measured EL intensity of μC B1 device is plotted as a function of wavelength and observation angle from 0° to 80° with normal direction of substrate.

2.3. Narrow Linewidth MOLEDs with Nonquarterwave DBRs

To further improve the spectral purity and investigate the modulation characteristics of MOLEDs, ultra-narrow deep blue emission has been demonstrated through the effects of microcavity modulation using nonquarterwave structural design. According to Equation (4), the spectral FWHM can be further reduced by increasing the reflectivity of the mirror or the effective cavity length. Only limited studies have been reported about a narrow-band organic EL emission of less than 3 nm driven electrically with optical microcavity.[25,45] Since the reflectivity of the common Al metal electrode is about 91% in the

Table 1. Summary of quarterwave blue MOLEDs performances.

Devices	Peak [nm]	Turn-on voltage [V]	Luminance$_{max}$ [cd m^{-2})]	[a)]EQE$_{max}$ [%]	[b)]FWHM [nm]
B0	434, 462	3.01 ± 0.04	23 000 ± 100 @11.6 V	4.95 ± 0.05 @5.22 cd m^{-2}	56 ± 1
μC B1	462	3.02 ± 0.05	19 800 ± 90 @15.7 V	8.86 ± 0.04 @8.02 cd m^{-2}	18 ± 0.5
μC B2	462	3.04 ± 0.05	8268 ± 68 @17.3 V	7.33 ± 0.06 @4.53 cd m^{-2}	10 ± 0.3
μC B3	462	3.03 ± 0.05	5120 ± 48 @16.2 V	3.24 ± 0.03 @2.03 cd m^{-2}	8 ± 0.2

[a)]EQE: external quantum efficiency; [b)]FWHM: full-width at half-maximum.

visible light band, according to the design principle of high-efficiency microcavity OLED, the reflectivity of the back mirror is higher than the light-output mirror. The reflectivity of the light-output mirror in the microcavity B3 device is close to 90%, while the spectral FWHM of the B1 device is only 8 ± 0.2 nm. A further improvement in the reflectivity of the light-output mirror cannot significantly reduce the spectral FWHM of the microcavity device, but at the same time, it may cause a significant decrease in the device performance. By increasing the thickness of the functional layer in the cavity, the effective cavity length can be increased to one wavelength, but is limited by the low mobility of the organic material, if the positive-intrinsic-negative doping method is not used, the electrical performance of the device could decrease significantly, which considerably increases the difficulty of the preparation process of the device. Moreover, theoretically, the spectral FWHM can only be reduced to 5–6 nm based on the method as mentioned above. We propose the idea of using a nonquarterwave microcavity design. The nonquarterwave microcavity refers to adjusting the length of the cavity through changing the penetration depth of the mirror or using the optical properties of the spacer in the microcavity. It does not modify the existing structural parameters of OLED, and thus it can maintain the carrier injection balance to the maximum extent. By using the nonquarterwave microcavity structure, it also offers a new way of fine-tuning the center position of exciton recombination and enhancing the coupling of excitons and standing wave light fields. This provides a systematic study on the luminescence dynamics process of the MOLEDs. To investigate the optical and electrical properties of nonquarterwave microcavities, MOLEDs were fabricated on nonquarterwave DBRs substrates with different spacer thicknesses. The microcavity devices with nonquarterwave DBR consist of 3.5 pairs of TiO_2/SiO_2, 0.5 λ_B nm SiO_2, and an ITO layer (DBRI), nonquarterwave DBR consists of 4.5 pairs of TiO_2/SiO_2, 0.5 λ_B nm SiO_2, and an ITO layer (DBRII), nonquarterwave DBR consists of 4.5 pairs of TiO_2/SiO_2, λ_B nm SiO_2, and an ITO layer (DBRIII), and nonquarterwave DBR consists of 4.5 pairs of TiO_2/SiO_2, 1.5 λ_B nm SiO_2, and an ITO layer (DBRIV), which led to the development of μC BI, μC BII, μC BIII, and μC BIV devices, respectively. The schematic illustration and the cross-sectional SEM of μC BIV device are shown in **Figure 4**a. The other cross-section SEM images of μC BI, μC BII, and μC BIII devices are shown in Figure S5 in the Supporting Information. The cross-section SEM investigations demonstrate the microstructure of nonquarterwave microcavity. Layers of amorphous organic and inorganic films were deposited with specific parameters as indicated in the fabrication methods. The nonquarterwave DBRs showed a homogenous amorphous SiO_2 structure with a sharp interface to the neighboring TiO_2 and ITO layers. It is beneficial to reduce optical loss and improve the quality factor of the microcavity. The reflectance of nonquarterwave DBRs is calculated by using the transfer matrix method, which presents that the reflectivity around 460 nm varies periodically with an increase in the spacer thickness (Figure 4b). Theoretically, the spacer layer can effectively adjust the length of the microcavity without substantially altering the reflection characteristics of DBR. The image of the μC BIII device displays a saturated blue light with apparent intensity distribution (Figure 4c). **Figure 5**a shows the *J*–*V*–*R* characteristics of microcavity devices with different nonquarterwave DBRs. It could be noted that the *J*–*V* characteristics of the devices are very similar, indicating that the electrical injection characteristics of the microcavity devices are not significantly affected by changing the structure of the device. The turn-on voltage of all MOLEDs is around 3.05 V. As the spectral linewidth of the microcavity devices is too narrow and the luminous wavelength is located in the blue region, the luminance cannot accurately reflect the output characteristics of the devices, and hence irradiance is used to characterize the output power of the microcavity devices. The μC BIV device shows the highest irradiance of 34.5 ± 0.45 mW cm^{-2}. Figure 5b exhibits EQE for the microcavity devices as a function of irradiance. The efficiency roll-off trend of μC BII, μC BIII, and μC BIV devices are similar, except for μCBI device. With an increase in the *Q* value and effective cavity length of the microcavity, EQE of the microcavity devices should decrease gradually. The μC BIV device having the longest cavity length shows the lowest EQE of 1.72 ± 0.02%. This phenomenon can be attributed to a gradual enhancement in the luminescence peak of the long cavity device in the green band. Figure 5c displays the normalized EL spectra of MOLEDs with different nonquarterwave DBRs. With a significant reduction in FWHM from 5.13 ± 0.15 to 2 ± 0.05 nm, the spectral FWHM decreases from μC BI to μC BIV devices, which is the narrowest spectral FWHM in blue to date (Table S2, Supporting Information). However, due to the additional EL peak at ≈550 nm, if such microcavity devices are to be used in the sensing applications, further suppression or reduction of emission intensity near 550 nm must be considered. With an increase in the thickness of the spacer, the spectra of microcavity devices can be significantly narrowed. This is due to that the effective length of the microcavity is gradually increased from 1/2 λ to 2 λ by increasing the thickness of the spacer layer with low absorption (**Table 2**). According to Equation (4), the spectral FWHM of the microcavity devices is considerably narrowed. Figure 5d shows the measured reflectivity of the microcavity devices from the normal direction of the bottom DBR. The μC BI, μC BII, μC BIII, and μC BIV devices with optimized structural design have almost the same resonance peak around 462 nm. In addition to a noticeable dip at the resonant peak position, there is no sudden change in the reflectivity of other regions. In nonquarterwave DBR, there are dips and the wavelength of which is distinct from that of the

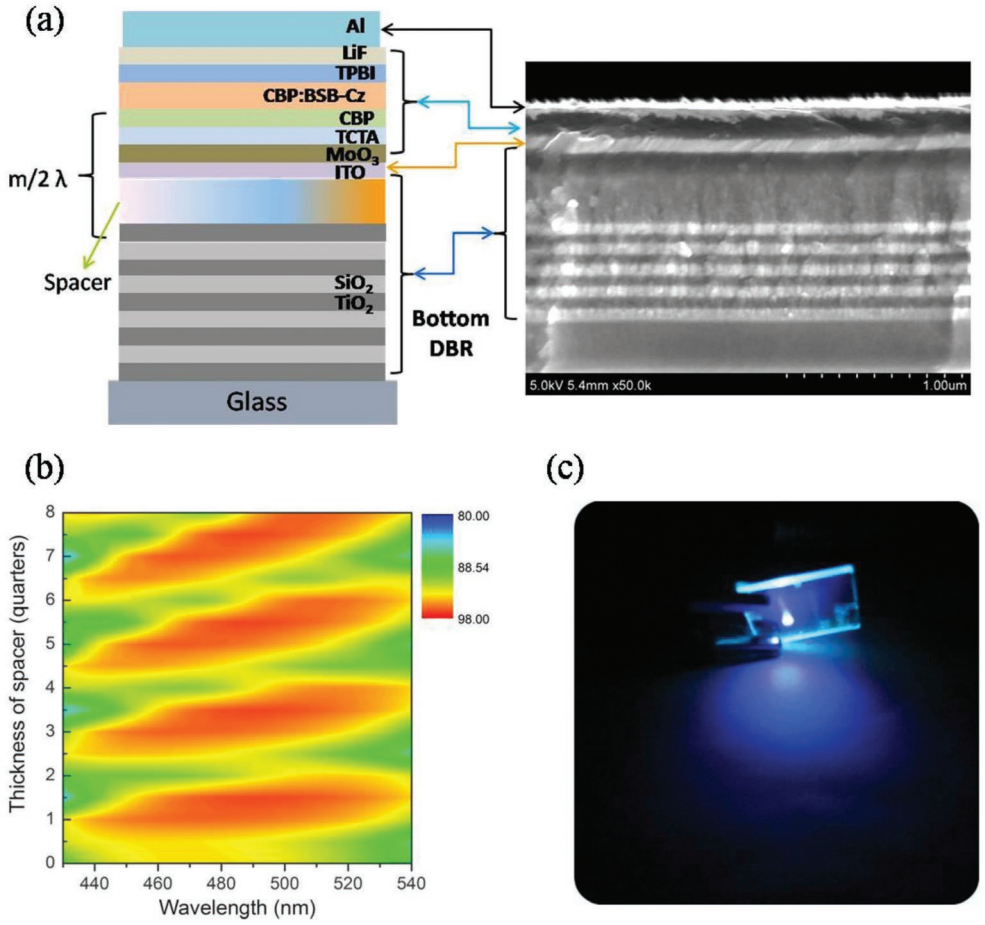

Figure 4. a) The structure diagram and cross-section SEM image of MOLEDs. b) The theoretical contour plot of the reflectance of nonquarterwave DBRs as the function of wavelength and spacer thickness. c) Image of μC BIII device at driving voltage of 6 V.

resonant wavelength in the region with higher reflectivity (Figure S6, Supporting Information), which does not affect the overall performance of the microcavity devices. This also experimentally proves that the actual interface for calculating the cavity length of the microcavity is not actually from the outermost layer of DBR. The cavity resonance bandwidths of μC BI, μC BII, μC BIII, and μC BIV devices tend to decrease gradually, indicating that the *Q* value of the corresponding device is steadily increasing. This corresponds to the gradual narrowing of the spectral FWHM of the devices, as mentioned earlier. The general operating principle of the optical microcavity with nonquarterwave DBR is shown in Figure 5e. By taking the metal dielectric microcavity, e.g., the fundamental difference between a conventional microcavity and nonquarterwave microcavity is that the nonquarterwave microcavity can realize the flexible regulation of the intracavity illumination mode by changing the thickness of the spacer layer. In theory, the thickness of the spacer layer can be irregular, which is determined by the thickness of the functional layer in the cavity and is optimized by the structure of the light-emitting device. The total thickness of the spacer and functional layers should satisfy the resonance condition of the microcavity. It is worth noting that the actual interface for calculating the cavity length of the microcavity does not start from the outermost layer of DBR (transparent conducting layer), but from the one with the highest reflectivity of DBR (underlying layer of the spacer layer). This design idea is very competitive for light-emitting devices with unbalanced carrier injection, such as QLEDs and perovskite light-emitting diodes (PeLEDs). The μC BIV device has shown good stability without packaging, indicating that the key difficulties in future practical applications can be effectively solved (Figure 5f). The angular resolution spectra of the microcavity devices with nonquarterwave DBRs are shown in Figure S7 in the Supporting Information, indicating strong forward emission distribution and blue shift with an increase in viewing angle at resonant and leakage modes, and the intensity ratio of the resonant and leakage modes decreases with an increase in the observation angle.

3. Conclusion

In this study, by using a nonquarterwave structural design, it has been found that MOLEDs possess tunable spectral FWHM as narrow as 2 ± 0.05 nm, and the spectral purity of MOLED is significantly enhanced. For blue OLEDs, the peak EQE reaches 5.19 ± 0.05% at 4.55 V with color-saturated blue

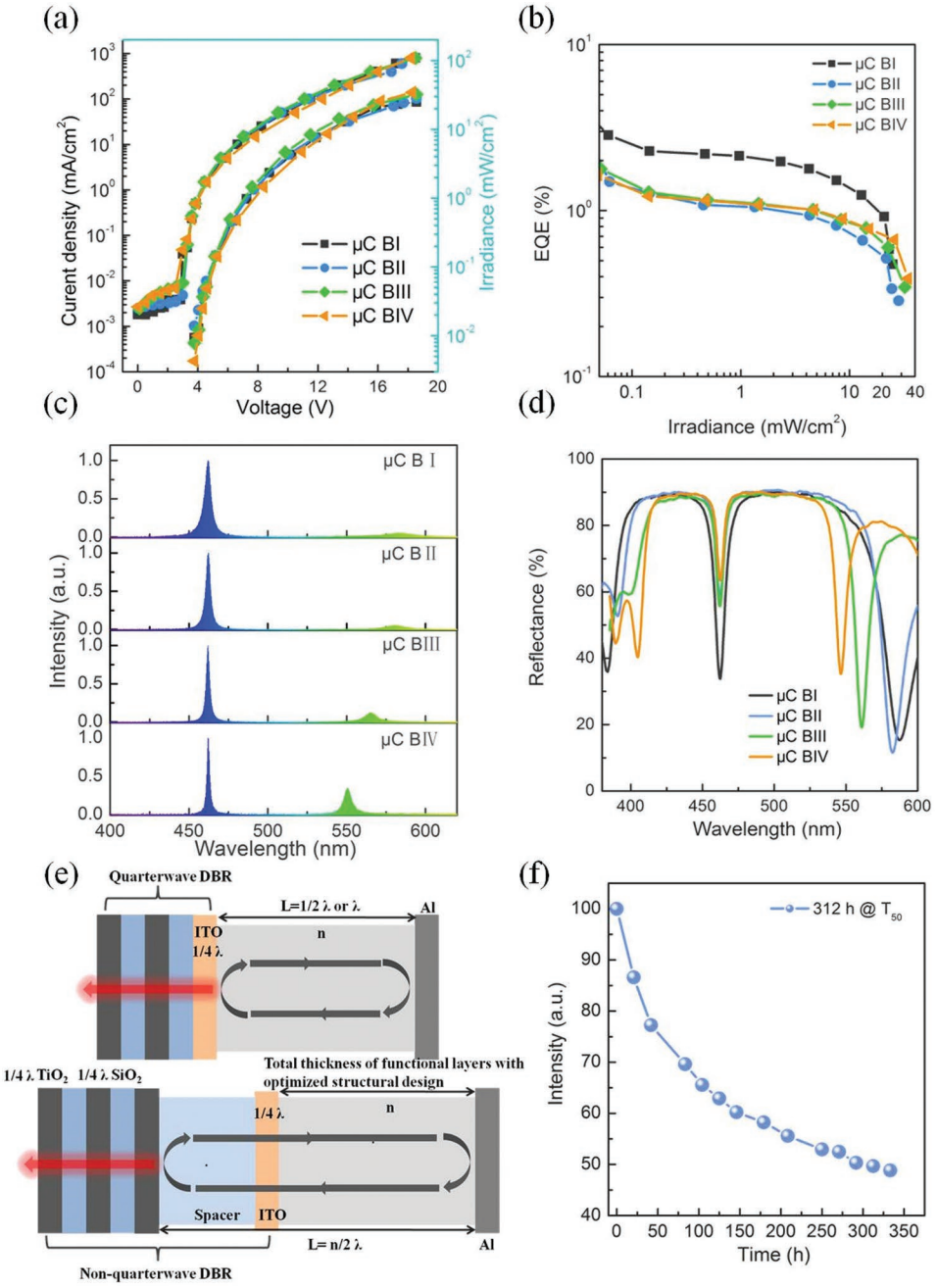

Figure 5. Performance of blue MOLEDs with nonquarterwave DBRs. a) *J–V–R* characteristics. b) EQE versus irradiance characteristics of the devices. c) EL spectra of MOLEDs with different nonquarterwave DBRs. d) The measured reflectance spectra of nonquarterwave MOLEDs from the normal direction of substrate. e) Schematic illustration of metal dielectric microcavity with different DBRs. Schematic of a Fabry–Perot resonator consisting of metal mirror and quarterwave DBR or nonquarterwave DBR are illustrated in upper and lower sides of the figure, surrounding a cavity medium of refractive index *n* and thickness *L*. f) The lifetime of the μC BIV device without encapsulation under EL peak of 462 nm and output power of 0.05 mW cm^{-2}.

emission (CIE: 0.14, 0.08). At the same time, the EQE of quarterwave MOLEDs is increased by 79% as compared to the reference device, and the narrowest FWHM is only 8 ± 0.2 nm. Also, through a careful designing of the optical cavity, highly efficient monochrome nonquarterwave MOLEDs have been built, which display a narrower FWHM of 2 ± 0.05 nm. These findings suggest that the followed strategy is powerful to tune the color purity for emitters with a large FWHM, such as emitters relying on organic materials, QD, or perovskite materials, which aim at achieving large area monochrome light source. Through these observations, the future of MOLEDs likely involves new materials and applications as compared to the currently employed in lighting and display systems. Also, it is expected that MOLEDs will be a competitor to conventional OLEDs and other forms of devices.

Table 2. Summary of nonquarterwave MOLEDs performances.

Devices	Peak [nm]	Turn-on voltage [V]	Irradiance$_{Max}$ [mW cm^{-2}]	EQE [%]	Spacer thickness [nm]	FWHM [nm]
μC BI	462	3.05 ± 0.04	25.1 ± 0.26 @18.5 V	3.86 ± 0.04 @0.039 mW cm^{-2}	164 ± 2	5.13 ± 0.15
μC BII	462	3.04 ± 0.05	28.3 ± 0.36 @18.5 V	2.35 ± 0.03 @0.045 mW cm^{-2}	164 ± 2	4.0 ± 0.1
μC BIII	462	3.06 ± 0.06	32.2 ± 0.42 @18.5 V	2.32 ± 0.03 @0.037 mW cm^{-2}	328 ± 4	2.8 ± 0.08
μC BIV	462	3.05 ± 0.05	34.5 ± 0.40 @18.2 V	1.72 ± 0.02 @0.025 mW cm^{-2}	492 ± 5	2 ± 0.05

4. Experimental Section

Materials: Titanium dioxide (TiO_2, 99%), silicon dioxide (SiO_2, 99%), TCTA (99%, EL device grade), CBP (99%, EL device grade), BSB-Cz (99%, EL device grade), and TPBI (99%, EL device grade) were purchased from Sigma Aldrich. All materials were used without further purification.

DBR Fabrication: The quarterwave DBR was consisted of several pairs of TiO_2/SiO_2 and an ITO layer with a λ_B of 480 nm. The TiO_2, SiO_2, and ITO films were deposited by electron beam evaporation at a substrate temperature of 280 °C and an oxygen pressure of 2.6×10^{-2} Pa. The optical thickness of TiO_2/SiO_2 and an ITO is 120 nm. The nonquarterwave DBR was consisted of several pairs of TiO_2/SiO_2 and TiO_2, then a spacer with low absorption, outermost layer was an ITO layer. The optical thickness of TiO_2/SiO_2 and an ITO was 120 nm, while the optical thickness of spacer was usually an integer multiple of 1/4 λ_B.

Fabrication of Blue OLEDs and MOLEDs: The custom-made ITO electrodes on glass substrates with resistance ≈60 Ω per □ were cleaned in deionized water, acetone, alcohol, and isopropanol consecutively with ultrasonic baths for 15 min each, and then treated with oxygen plasma for 2–3 min. All organic layers were sequentially deposited onto the substrate at 3×10^{-4} Pa using vacuum thermal evaporation deposition. The deposition rates were controlled from 0.15 to 0.25 nm s^{-1} for organic materials and 0.01 nm s^{-1} for molybdenum trioxide (MoO_3) and lithium fluorine (LiF). Finally, the aluminum cathode was deposited at a rate of 1–2 nm s^{-1}. The deposition rates were controlled in situ with a quartz crystal monitor and corrected by footstep machine simultaneously. The MOLEDs with patterned ITO electrodes (≈60 Ω per □) were constructed with the same procedures as abovementioned.

Characterizations: Absolute fluorescent quantum yield measurements were carried out using a calibrated integrating sphere on the Edinburgh FLS920 spectrometer. The thickness of the films was calibrated using a surface profiler (XP-1, Ambios). The reflectance spectra of the DBRs were measured using a UV-visible-near-IR spectrophotometer (Lambda 1050, PerkinElmer). The current density–voltage (*J*–*V*) characteristics of the devices were determined using a computer-controlled Keithley 2611 source meter. The EL spectra and luminance of the OLEDs were obtained using a well-calibrated Spectroradiometer (PR 705, Photo Research) and cross-checked with a fiber spectrometer (AvaSpec USB 3648, Avantes). The devices had emission areas of 1 × 1 mm^2. Irradiance–current–voltage curves were measured using a system incorporating a powermeter (PM320E, Thorlabs) and a source-measure unit (2611, Keithley). The method of direct measurement of EQE[46,47] was performed by using a high sensitivity (5 nW to 0.5 mW), large diameter detector (S130 VC, Thorlabs, ∅9.5 mm) to measure the output power of devices, making sure the detector in contact with the active pixel as much as possible and the device under test underfilled the detector area, while monitoring the current simultaneously. The EQE was calculated by converting the power signal to emit photons and the device current to electrons. All characterizations were conducted at room temperature in the ambient environment.

Supporting Information

Supporting Information is available from the Wiley Online Library or from the author.

Acknowledgements

This work was financially supported by the cooperation Fund between CIOMP and FuDan University, the National Natural Science Foundation of China nos. 61975256, 51973208, 61774154, 61704170, 61875195, and 61775211, the Jilin Province Science and Technology Research Project nos. 20180201029GX, 20170101039JC, 20190302087GX, and 20190302084GX, and financial support from the State Key Laboratory of Luminescence and Applications, and Dawn Talent Training Program of CIOMP, and this work was also supported by Youth Innovation Promotion Association CAS (2019225), the Open Fund of the State Key Laboratory of Luminescent Materials and Devices (South China University of Technology, 2019-skllmd-07).

Conflict of Interest

The authors declare no conflict of interest.

Keywords

blue emission, nonquarterwave microcavities, organic light-emitting diodes, spectral linewidth, structural design

Received: August 20, 2019
Revised: December 5, 2019
Published online: January 17, 2020

[1] C. W. Tang, S. A. VanSlyke, *Appl. Phys. Lett.* **1987**, *51*, 913.
[2] M. A. Baldo, D. F. O'Brien, Y. You, A. Shoustikov, S. Sibley, M. E. Thompson, S. R. Forrest, *Nature* **1998**, *395*, 151.
[3] M. G. Helander, Z. B. Wang, J. Qiu, M. T. Greiner, D. P. Puzzo, Z. W. Liu, Z. H. Lu, *Science* **2011**, *332*, 944.
[4] H. Uoyama, K. Goushi, K. Shizu, H. Nomura, C. Adachi, *Nature* **2012**, *492*, 234.
[5] J. W. Sun, J.-H. Lee, C. K. Moon, K. H. Kim, H. Shin, J.-J. Kim, *Adv. Mater.* **2014**, *26*, 5684.
[6] H. Nakanotani, T. Higuchi, T. Furukawa, K. Masui, K. Morimoto, M. Numata, H. Tanaka, Y. Sagara, T. Yasuda, C. Adachi, *Nat. Commun.* **2014**, *5*, 4016.
[7] Y. F. Liu, J. Feng, Y. G. Bi, D. Yin, H. B. Sun, *Adv. Mater. Technol.* **2019**, *4*, 1800371.

[8] H. W. Chen, J. H. Lee, B. Y. Lin, S. Chen, S. T. Wu, *Light: Sci. Appl.* **2018**, *7*, 17168.
[9] J. H. Lee, C. H. Chen, P. H. Lee, H. Y. Lin, M. Leung, T. L. Chiu, C. F. Lin, *J. Mater. Chem. C* **2019**, *7*, 5874.
[10] X. Dai, Z. Zhang, Y. Jin, Y. Niu, H. Cao, X. Liang, L. Chen, J. Wang, X. Peng, *Nature* **2014**, *515*, 96.
[11] C. R. Kagan, E. Lifshitz, E. H. Sargent, D. V. Talapin, *Science* **2016**, *353*, aac5523.
[12] X. Dai, Y. Deng, X. Peng, Y. Jin, *Adv. Mater.* **2017**, *29*, 1607022.
[13] H. Shen, Q. Gao, Y. Zhang, Y. Lin, Q. Lin, Z. Li, L. Chen, Z. Zeng, X. Li, Y. Jia, S. Wang, Z. Du, L. S. Li, Z. Zhang, *Nat. Photon.* **2019**, *13*, 192.
[14] O. Ostroverkhova, *Chem. Rev.* **2016**, *116*, 13279.
[15] W. C. Tien, L. Y. Chen, Y. W. Zeng, K. W. Chang, A. K. Chu, *Electron. Lett.* **2015**, *51*, 2034.
[16] E. Manna, F. Fungura, R. Biswas, J. Shinar, R. Shinar, *Adv. Funct. Mater.* **2015**, *25*, 1226.
[17] R. Liu, Y. Cai, J.-M. Park, K.-M. Ho, J. Shinar, R. Shinar, *Adv. Funct. Mater.* **2011**, *21*, 4744.
[18] C. Grivas, M. Pollnau, *Laser Photonics Rev.* **2012**, *6*, 419.
[19] S. R. Park, M. C. Suh, *Opt. Express* **2018**, *26*, 4979.
[20] R. G. Baets, D. Delbeke, R. Bockstaele, P. Bienstman, *Proc. SPIE* **2003**, *4996*, 74.
[21] A. J. Shaw, A. L. Bradley, J. F. Donegan, J. G. Lunney, *IEEE Photonics Technol. Lett.* **2004**, *16*, 2006.
[22] C. Medina, M. Zambrano Nuñez, K. Navarro, *Int. J. Adv. Eng. Technol.* **2015**, *8*, 482.
[23] S. Kwon, E.H. Lee, K. Kim, H. Choi, M. J. Park, S. K. Kim, R. Pode, J. H. Kwon, *Opt. Express* **2017**, *25*, 29906.
[24] C. Xiang, W. Koo, F. So, H. Sasabe, J. Kido, *Light: Sci. Appl.* **2013**, *2*, e74.
[25] A. Genco, G. Giordano, S. Carallo, G. Accorsi, Y. Duan, S. Gambino, M. Mazzeo, *Org. Electron.* **2018**, *62*, 174.
[26] M. Wang, J. Lin, Y.C. Hsiao, X. Liu, B. Hu, *Nat. Commun.* **2019**, *10*, 1614.
[27] C. Lin, H. W. Lin, C. C. Wu, *Appl. Phys. Lett.* **2005**, *87*, 021101.
[28] M. Sarma, K. T. Wong, *Chem. Rec.* **2019**, *19*, 1667.
[29] J. Tagare, S. Vaidyanathan, *J. Mater. Chem. C* **2018**, *6*, 10138.
[30] C.-Y. Chan, M. Tanaka, H. Nakanotani, C. Adachi, *Nat. Commun.* **2018**, *9*, 5036.
[31] J. Lee, C. Jeong, T. Batagoda, C. Coburn, M. E. Thompson, S. R. Forrest, *Nat. Commun.* **2017**, *8*, 15566.
[32] N. A. Kukhta, T. Matulaitis, D. Volyniuk, K. Ivaniuk, P. Turyk, P. Stakhira, J. V Grazulevicius, A. P. Monkman, *J. Phys. Chem. Lett.* **2017**, *8*, 6199.
[33] M. Mamada, T. Fukunaga, F. Bencheikh, A. S. D. Sandanayaka, C. Adachi, *Adv. Funct. Mater.* **2018**, *28*, 1802130.
[34] H. Etori, T. Yasuda, X. L. Jin, K. Fujita, S. Mataka, T. Tsutsui, *Jpn. J. Appl. Phys.* **2007**, *46*, 5071.
[35] Y. Yang, P. Cohn, S.H. Eom, K. A. Abboud, R. K. Castellano, J. G. Xue, *J. Mater. Chem. C* **2013**, *1*, 2867.
[36] N. Takada, T. Tsutsui, S. Saito, *Appl. Phys. Lett.* **1993**, *63*, 2032.
[37] R. H. Jordan, L. J. Rothberg, A. Dodabalapur, R. E. Slusher, *Appl. Phys. Lett.* **1996**, *69*, 1997.
[38] A. Dodabalapur, L. J. Rothberg, R. H. Jordan, T. M. Miller, R. E. Slusher, J. M. Phillips, *J. Appl. Phys.* **1996**, *80*, 6954.
[39] M. G. Helander, Z. B. Wang, M. T. Greiner, Z. W. Liu, J. Qiu, Z. H. Lu, *Adv. Mater.* **2010**, *22*, 2037.
[40] N. E. J. Hunt, E. F. Schubert, R. F. Kopf, D. L. Sivco, A. Y. Cho, G. J. Zydzik, *Appl. Phys. Lett.* **1993**, *63*, 2600.
[41] E. F. Schubert, *Light-Emitting Diodes*, Cambridge University Press, Cambridge **2006**.
[42] X. Liu, H. Li, C. Song, Y. Liao, M. Tian, *Opt. Lett.* **2009**, *34*, 503.
[43] J. Lin, Y. Hu, Y. Lv, X. Guo, X. Liu, *Sci. Bull.* **2017**, *62*, 1637.
[44] J. Shinar, R. Shinar, *J. Phys. D: Appl. Phys.* **2008**, *41*, 133001.
[45] W. Shen, J. Wang, H. Chen, H. Li, X. Liu, P. Gu, *Acta Photonica Sin.* **2004**, *33*, 155.
[46] S. R. Forrest, D. D. C. Bradley, M. E. Thompson, *Adv. Mater.* **2003**, *15*, 1043.
[47] C. Song, N. Zhang, J. Lin, X. Guo, X. Liu, *Sci. Rep.* **2017**, *7*, 41250.

